coordination sites based solely on coordination bond distances.

The bond distances and angles associated with the coordinated DiPDECMP ligand in **1** are typical of those found in $UO_2(NO_3)_2$(DiPDECMP) (**8**), $Th(NO_3)_4$(DEDECMP)$_2$ (**9**), and $Sm(NO_3)_3$(DiPDECMP)$_2$ (**10**). The phosphoryl bond distance P(1)-O(1), 1.487 (2) Å, compares with distances in **8** (1.485 (5) Å), **9** (1.478 (4) Å), and **10** (1.480 (2) Å) as well as with the distances in the monodentate phosphoryl complex **2** (1.492 (1) Å). The corresponding distances in **6** are much shorter: 1.457 (4) and 1.437 (4) Å. The carbonyl bond distance C(2)-O(4), 1.262 (3) Å, in **1** is also similar to those found in **8** (1.260 (8) Å), **9** (1.256 (6) Å), and **10** (1.261 (3) Å). The corresponding distances in other Mo(VI)-carbonyl complexes show greater variability: **3**, 1.233 (4) Å and 1.235 (4) Å; **4**, 1.29 (1) Å. The bond angles about P(1), C(1), and C(2) compare well with the angles found in **8**, **9**, and **10**.

The isolation, characterization, and single-crystal X-ray structure determination for **1** indicate that in the solid state this complex contains a single DiPDECMP ligand bonded in a cis-bidentate configuration to MoO_2Cl_2. The composition and structure of the species formed in solution during the extraction of MoO_2Cl_2 by CMP ligands are under investigation in our group at this time.

Acknowledgment. R.T.P. wishes to recognize financial support for this work from the Department of Energy, Office of Basic Energy Sciences, Contract No. 81ER-10465. He also wishes to recognize NSF Grant CHE-7802921, which facilitated the purchase of the X-ray diffractometer.

Supplementary Material Available: Listings of structure factors, hydrogen atom positional parameters, and thermal parameters (13 pages). Ordering information is given on any current masthead page.

Contribution from the Department of Chemistry, The University of North Carolina at Chapel Hill, Chapel Hill, North Carolina 27514

Crystal Structures and Magnetic and EPR Studies of Intradimer and Interdimer Exchange Coupling in $[M(en)_3]_2[Cu_2Cl_8]Cl_2\cdot 2H_2O$ (M = Co, Rh, Ir) Crystals

S. K. HOFFMANN,[1] DEREK J. HODGSON, and WILLIAM E. HATFIELD*

Received June 29, 1984

Single-crystal EPR measurements and magnetic susceptibility data are presented for the compounds $[M(C_2H_8N_2)_3]_2[Cu_2Cl_8]Cl_2\cdot 2H_2O$ (M = Co (I), Rh (II), Ir (III); $C_2H_8N_2$ = ethylenediamine, en). The crystal and molecular structures of $[M(en)_3]_2[Cu_2Cl_8]Cl_2\cdot 2H_2O$ (M = Rh (II), Ir (III)) have been determined from single-crystal, three-dimensional X-ray diffraction counter data. The compounds crystallize as orange prisms in space group *Pbca* with $Z = 4$ and have unit cell dimensions of $a = 13.639$ (6) Å, $b = 14.577$ (11) Å, and $c = 18.020$ (6) Å for the rhodium compound and $a = 13.705$ (5) Å, $b = 14.467$ (19) Å, and $c = 18.091$ (6) Å for the iridium compound. The structures were refined by full-matrix least-squares techniques to R values of 0.036 for the rhodium compound and 0.049 for the iridium compound. The compounds are isomorphous with $[Co(en)_3]_2[Cu_2Cl_8]Cl_2\cdot 2H_2O$. The crystal structure consists of layers of magnetically inequivalent $Cu_2Cl_8^{4-}$ dimers with antiferromagnetic intradimer coupling $2J = -14.6$ cm^{-1} in I, -13.8 cm^{-1} in II, and -13.0 cm^{-1} in III. The dimers are well separated by large $[M(en)_3]^{3+}$ diamagnetic complexes. The hyperfine and fine structures are not resolved in the EPR spectra. The spectra are partially averaged by interdimer exchange interaction and indicate a strong merging effect of the EPR lines. The EPR spectral parameters were determined by computer simulation using solutions to the generalized Bloch equations. Molecular g factors have been found to be similar in all three compounds with $g_z = 2.290$, $g_y = 2.020$, and $g_x = 2.116$ in II. From the simulation procedure the values of the interdimer exchange integrals between neighbor layers have been found to be 0.007 12 cm^{-1} in I, 0.001 35 cm^{-1} in II, and 0.001 90 cm^{-1} in III at room temperature. This weak exchange coupling decreases linearly with temperature and reaches values of 0.003 14 cm^{-1} in I, 0.000 70 cm^{-1} in II, and 0.000 52 cm^{-1} in III at 77 K. This is a result of decreases in overlaps between atomic orbitals in the superexchange pathways with decreases of the average amplitudes of thermal lattice vibrations.

Introduction

Magnetostructural correlations in hydroxo-bridged,[2,3] alkoxo-bridged,[4] chloro-bridged,[5,6] bromo-bridged,[6] and sulfur-bridged[6,7] copper(II) dimers are well documented experimentally. The dimeric unit $[Cu_2Cl_8]^{4-}$ in $[Co(en)_3]_2[Cu_2Cl_8]Cl_2\cdot 2H_2O$ obeys the predicted[5,6] relationship between singlet-triplet splitting $2J$ and the quotient ϕ/R_0 (ϕ = bridge angle, R_0 = longest bridge arm) with $2J = -14.6$ cm^{-1} [7] and $\phi/R_0 = 35.2°$ Å^{-1}.[8,9] The $2J$, ϕ/R_0 dependence is very sensitive to small changes in the bridge geometry. Thus, a substitution for the Co(III) ion in $[Co(en)_3]_2[Cu_2Cl_8]Cl_2\cdot 2H_2O$ by ions with larger ionic radii, such as Rh(III) or Ir(III), should result in small changes in ϕ/R_0 from the influence of the size of the cation on the crystal packing.

We have previously reported[9] the crystal structure of $[Co(en)_3]_2[Cu_2Cl_8]Cl_2\cdot 2H_2O$, and the structures of the Rh(III) and Ir(III) complexes are shown here to be isomorphous. EPR powder spectra of the compounds, recorded at both room temperature and 77 K, are unusual since absorptions appear from both averaged and nonaveraged EPR lines of magnetically nonequivalent copper(II) complexes in the unit cell. This observation strongly suggests an interdimer interaction with a coupling strength in the range that can be observed by EPR spectroscopy. The EPR lines from nonequivalent complexes are perturbed by this interaction, and EPR spectral parameters cannot be determined directly from recorded EPR spectra. The interpretation of the EPR spectra of $[Co(en)_3]_2[Cu_2Cl_8]Cl_2\cdot 2H_2O$[10-12] has been refined to take this effect into account, and the spectra of the Rh(III) and Ir(III) analogues are also presented and interpreted in terms of temperature-dependent interdimer interactions.

Experimental Section

Electron Paramagnetic Resonance. EPR spectra were recorded with a Varian E-109 spectrometer at X-band. The microwave frequency was monitored with a Hewlett-Packard 5245L frequency counter, and the

(1) Permanent address: Institute of Molecular Physics, Polish Academy of Sciences, 60-179 Poznan, Poland.
(2) Crawford, V. H.; Richardson, H. W.; Wasson, J. R.; Hodgson, D. J.; Hatfield, W. E. *Inorg. Chem.* **1976**, *15*, 2107.
(3) Hatfield, W. E. In "Theory and Applications of Molecular Paramagnetism"; Boudreaux, E. A., Mulay, L. N., Eds.; Wiley: New York, 1976; Chapter 7.
(4) Morgehenn, R.; Merz, L.; Haase, W. *J. Chem. Soc., Dalton Trans.* **1980**, 1703.
(5) Marsh, W. E.; Patel, K. C.; Hatfield, W. E.; Hodgson, D. J. *Inorg. Chem.* **1983**, *22*, 511.
(6) Hatfield, W. E. *Comments Inorg. Chem.* **1981**, *1*, 105.
(7) Hatfield, W. E. *Inorg. Chem.* **1983**, 22, 833.
(8) McGregor, K. T.; Losee, D. B.; Hodgson, D. J.; Hatfield, W. E. *Inorg. Chem.* **1974**, *13*, 756.
(9) Hodgson, D. J.; Hale, P. K.; Hatfield, W. E. *Inorg. Chem.* **1971**, *10*, 1061.
(10) Hoffmann, S. K.; Hatfield, W. E. *J. Magn. Reson.* **1983**, *53*, 341.
(11) McGregor, K. T.; Hatfield, W. E. *J. Chem. Phys.* **1976**, *65*, 4155.
(12) McGregor, K. T.; Hatfield, W. E. *J. Chem. Phys.* **1975**, *62*, 2911.

0020-1669/85/1324-1194$01.50/0

Table I. Crystallographic Parameters for $[M(en)_3]_2[Cu_2Cl_8]Cl_2 \cdot 2H_2O$

	M = Co[a]	M = Rh	M = Ir
a, Å	13.560 (9)	13.639 (6)	13.705 (5)
b, Å	14.569 (9)	14.577 (11)	14.467 (19)
c, Å	17.885 (12)	18.020 (6)	18.091 (6)
V, Å^3	3533 (7)	3583 (6)	3587 (7)
space group	*Pbca*	*Pbca*	*Pbca*
Z	4	4	4
μ, cm^{-1}	29.75	28.67	98.09
range of transmission factors	0.675–0.763	0.785–0.993	0.253–0.999
NO ($>3\sigma(I)$)	1275	3023	2647
data range, deg	$2\theta < 45$	$2\theta < 55$	$2\theta < 55$
data collected	$+h,+k,+l$	$+h,+k,+l$,	$-h,+k,-l$
cryst shape and size, mm	hexagonal prism, 0.24 × 0.13	hexagonal prism, 0.41 × 0.20	hexagonal prism, 0.38 × 0.18
R_1	0.065	0.036	0.049
R_2	0.069	0.036	0.049

[a] Data from ref 9.

magnetic field was calibrated with a DPPH marker. Angular-dependent spectra of single crystals were recorded at room temperature and at 77 K around the crystallographic axes. The temperature dependences of the spectra along a, b, and c and along the z axis of the copper(II) complex were measured in the temperature range 77–370 K with a Varian E-4557 variable-temperature accessory.

Magnetic Susceptibility. Magnetic susceptibility data were collected in the temperature range 4.2–70 K on powdered and single-crystal samples with a PAR Model 155 vibrating-sample magnetometer, which was operated at 10 and 15 kG. The magnetometer was calibrated with $HgCo(SCN)_4$ and with a Ni sphere in a saturation field.[13,14] A calibrated GaAs diode was used to measure the temperature. The magnetic susceptibility data were corrected for the diamagnetism of constituent atoms and for temperature-independent paramagnetism.[15]

X-ray Data Collection and Reduction. (a) $[Rh(en)_3]_2[Cu_2Cl_8]Cl_2 \cdot 2H_2O$. A prismatic crystal was mounted on a glass fiber in an arbitrary orientation and placed on an Enraf-Nonius CAD4 automatic diffractometer. Preliminary examination confirmed that the crystals belong to the orthorhombic system and that they are isomorphous with the $[Co(en)_3]^{3+}$ salt.[9] Crystal data are compared with those of the $[Co(en)_3]^{3+}$ and $[Ir(en)_3]^{3+}$ salts in Table I.

Diffraction data were collected and corrected for absorption in the manner described previously.[16] A total of 4587 intensities, of which 3023 were independent data with $I > 3\sigma(I)$, was recorded with use of Mo Kα radiation (λ = 0.710 73 Å) at a temperature of 20 °C; only these latter data were used in the structure refinement.

(b) $[Ir(en)_3]_2[Cu_2Cl_8]Cl_2 \cdot 2H_2O$. Data collection, absorption correction, and reduction were carried out as described above. A total of 4570 intensities was recorded, yielding 2647 independent data with $I > 3\sigma(I)$.

Solution and Refinement of the Structures. The isomorphism of the complexes with the $[Co(en)_3]$ salt was verified by inspection of three-dimensional Patterson functions. The structures were then solved by entering the coordinates of the heavy atoms (Co, Cu, Cl) from the $[Co(en)_3]$ structure,[9] with Rh or Ir substituted for Co as appropriate. All least-squares calculations were carried out on F, the function minimized being $\sum w(|F_o| - |F_c|)^2$, where the weights w are assigned as $4F_o^2/\sigma^2(I)$ and $\sigma(I)$ is as described elsewhere.[16,17] The effects of the anomalous dispersion of all atoms were included.

$[Rh(en)_3]_2[Cu_2Cl_8]Cl_2 \cdot 2H_2O$. Refinement of the seven Rh, Cu, and Cl atoms gave values of $R_1 = \sum||F_o| - |F_c||/\sum|F_o|$ and $R_2 = [\sum w(|F_o| - |F_c|)^2/\sum wF_o^2]^{1/2}$ of 0.227 and 0.265, respectively. A subsequent difference Fourier map very clearly revealed the positions of the C, N, and O atoms, and eventual anisotropic refinement of all 20 non-hydrogen atoms yielded R_1 = 0.051 and R_2 = 0.064. The hydrogen atoms could all be unambiguously located in a difference Fourier map, but attempts to refine these positions were unsuccessful. Consequently, the ligand hydrogen atoms were placed in calculated positions based on tetrahedral geometry at C or N and C–H and N–H distances of 0.95 and 0.87 Å, respectively.[18] The water hydrogen atoms were included in the positions indicated by a difference Fourier summation after inclusion of the ligand hydrogen atoms. Ligand hydrogen atoms were assigned fixed isotropic thermal parameters B of 5.0 Å^2, while water hydrogen atoms were assigned B = 6.0 Å^2. In a final least-squares calculation, the non-hydrogen atoms were refined anisotropically but no hydrogen atom parameter was varied. The final cycle involved 3023 intensities and 181 variables and yielded values of 0.036 for both R_1 and R_2. No parameter shifted by more than 0.07σ, which indicates that the refinement had converged. A final difference Fourier showed some minor residual electron density of 0.35 e Å^{-3} in the vicinity of the Rh atom but was otherwise featureless. The refined atomic positional parameters, along with their estimated standard deviations, are listed in Table II. Listings of hydrogen atom positions, anisotropic thermal parameters, and observed and calculated structure amplitudes for both structures are available as supplementary material.

$[Ir(en)_3]_2[Cu_2Cl_8]Cl_2 \cdot 2H_2O$. Refinement was carried out as above, but the hydrogen atom positions were not all apparent in a difference Fourier map. The ligand hydrogen atoms were placed in calculated positions as before, but the water hydrogen atoms could not be located and were not included. The final least-squares cycle, calculated as above, involved 2647 observations and 181 variables and converged to values of 0.049 for

Table II. Atomic Positional Parameters for $[Rh(en)_3]_2[Cu_2Cl_8]Cl_2 \cdot 2H_2O$

atom	x	y	z
Rh	0.34112 (2)	0.17189 (2)	0.11270 (2)
Cu	−0.02697 (4)	−0.00830 (4)	0.10040 (3)
Cl(1)	0.13541 (8)	−0.02943 (8)	0.13362 (8)
Cl(2)	0.02032 (8)	0.11183 (8)	0.02408 (7)
Cl(3)	−0.17171 (8)	0.06247 (8)	0.12712 (8)
Cl(4)	−0.07449 (8)	−0.13445 (8)	0.16366 (7)
Cl(5)	0.09787 (8)	0.37743 (8)	0.07223 (7)
O	0.4652 (3)	0.2419 (3)	0.3334 (2)
N(1)	0.3054 (3)	0.0834 (2)	0.0265 (2)
N(2)	0.3109 (2)	0.2713 (2)	0.0341 (2)
N(3)	0.1985 (2)	0.1783 (2)	0.1481 (2)
N(4)	0.3619 (2)	0.2647 (2)	0.1976 (2)
N(5)	0.3803 (3)	0.0646 (2)	0.1826 (2)
N(6)	0.4894 (2)	0.1697 (3)	0.0875 (2)
C(1)	0.3099 (3)	0.1347 (3)	−0.0442 (3)
C(2)	0.2628 (3)	0.2268 (3)	−0.0311 (3)
C(3)	0.1984 (3)	0.2112 (3)	0.2259 (3)
C(4)	0.2664 (3)	0.2928 (3)	0.2306 (3)
C(5)	0.4884 (3)	0.0659 (3)	0.1929 (3)
C(6)	0.5351 (3)	0.0857 (3)	0.1194 (3)

Table III. Atomic Positional Parameters for $[Ir(en)_3]_2[Cu_2Cl_8]Cl_2 \cdot 2H_2O$

atom	x	y	z
Ir	0.34126 (2)	0.17224 (3)	0.11260 (2)
Cu	−0.02628 (8)	−0.00814 (9)	0.10005 (8)
Cl(1)	0.1357 (2)	−0.0294 (2)	0.1333 (2)
Cl(2)	0.0203 (2)	0.1120 (2)	0.0242 (2)
Cl(3)	−0.1710 (2)	0.0632 (2)	0.1273 (2)
Cl(4)	−0.0734 (2)	−0.1342 (2)	0.1639 (2)
Cl(5)	0.0973 (2)	0.3779 (2)	0.0721 (2)
O	0.4630 (6)	0.2436 (6)	0.3342 (5)
N(1)	0.3063 (6)	0.0838 (6)	0.0265 (5)
N(2)	0.3092 (6)	0.2720 (6)	0.0333 (5)
N(3)	0.1977 (6)	0.1788 (7)	0.1491 (6)
N(4)	0.3618 (5)	0.2652 (6)	0.1977 (6)
N(5)	0.3820 (6)	0.0645 (6)	0.1831 (5)
N(6)	0.4904 (6)	0.1697 (7)	0.0868 (5)
C(1)	0.3079 (8)	0.1353 (8)	−0.0452 (7)
C(2)	0.2619 (8)	0.2276 (8)	−0.0313 (7)
C(3)	0.1975 (7)	0.2118 (8)	0.2275 (7)
C(4)	0.2654 (7)	0.2926 (8)	0.2307 (8)
C(5)	0.4890 (8)	0.0662 (8)	0.1923 (7)
C(6)	0.5379 (8)	0.0869 (8)	0.1214 (7)

(13) Brown, D. B.; Crawford, V. H.; Hall, J. W.; Hatfield, W. E. *J. Phys. Chem.* **1977**, *81*, 1303.
(14) McKim, F. R.; Wolf, W. P. *J. Sci. Instrum.* **1957**, *34*, 64.
(15) Weller, R. R.; Hatfield, W. E. *J. Chem. Educ.* **1979**, *56*, 652.
(16) Graves, B. J.; Hodgson, D. J. *Acta Crystallogr., Sect. B: Struct. Crystallogr. Cryst. Chem.* **1982**, *38B*, 135.
(17) Corfield, P. W. R.; Doedens, R. J.; Ibers, J. A. *Inorg. Chem.* **1967**, *6*, 197.
(18) Churchill, M. R. *Inorg. Chem.* **1973**, *12*, 1213.

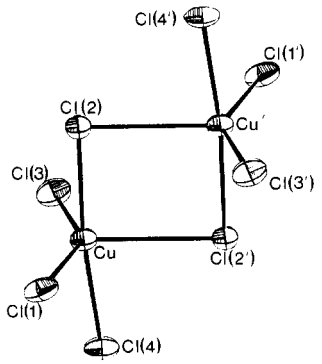

Figure 1. Geometry of $[Cu_2Cl_8]^{4-}$ in $[Rh(en)_3]_2[Cu_2Cl_8]Cl_2 \cdot 2H_2O$.

Table IV. Intramolecular Distances (Å) and Angles (deg) in the $[Cu_2Cl_8]^{4-}$ Ion in $[M(en)_3]_2[Cu_2Cl_8]Cl_2 \cdot 2H_2O$

atoms	M = Co[a]	M = Rh	M = Ir
Cu-Cu	3.722 (5)	3.700 (1)	3.699 (2)
Cu-Cl(1)	2.319 (5)	2.315 (1)	2.321 (2)
Cu-Cl(2)	2.325 (4)	2.318 (1)	2.305 (2)
Cu-Cl(2)'	2.703 (5)	2.705 (1)	2.705 (2)
Cu-Cl(3)	2.273 (5)	2.279 (1)	2.289 (2)
Cu-Cl(4)	2.262 (5)	2.259 (1)	2.254 (2)
Cl(1)-Cu-Cl(2)	89.2 (2)	89.30 (3)	89.40 (8)
Cl(1)-Cu-Cl(2)'	96.3 (2)	96.21 (3)	96.48 (8)
Cl(1)-Cu-Cl(3)	145.3 (2)	146.56 (4)	146.37 (9)
Cl(1)-Cu-Cl(4)	92.2 (2)	92.04 (3)	91.94 (8)
Cl(2)-Cu-Cl(2)'	84.8 (1)	85.42 (3)	85.17 (7)
Cl(2)-Cu-Cl(3)	91.9 (2)	91.40 (3)	91.59 (8)
Cl(2)-Cu-Cl(4)	172.6 (2)	173.88 (4)	174.27 (9)
Cl(2)'-Cu-Cl(3)	118.3 (2)	117.18 (3)	117.10 (8)
Cl(2)'-Cu-Cl(4)	87.8 (2)	88.50 (3)	89.14 (8)
Cl(3)-Cu-Cl(4)	91.1 (2)	90.76 (3)	90.38 (8)
Cu-Cl(2)-Cu'	95.2 (1)	94.58 (3)	94.83 (7)

[a] Data from ref 9.

both R_1 and R_2. No parameter experienced a shift of more than 0.6σ, indicating convergence. A final difference Fourier showed several peaks of up to 0.68 e Å^{-3} in the vicinity of the Ir atom, which presumably indicates some minor error in our absorption correction; such an error is not surprising in view of the large value of the absorption coefficient of this compound for Mo Kα radiation (see Table I). There were no chemically meaningful peaks, however. The refined atomic positional parameters are presented in Table III.

Results and Discussion

Descriptions of the Structures. The structures consist of dimeric $[Cu_2Cl_8]^{4-}$ ions, discrete Cl^- ions, $[M(en)_3]^{3+}$ (M = Rh, Ir) cations, and water molecules. The geometry of the $[Cu_2Cl_8]^{4-}$ moiety in the $[Rh(en)_3]^{3+}$ salt is shown in Figure 1, and the essential similarity of the geometries found for this unit in the three structures is confirmed by the comparison of bond lengths and angles presented in Table IV. The dimeric anion is best viewed as consisting of two bipyramidal units that share an edge; thus, the bridging atoms Cl(2) and Cl(2)′ are axial to one copper atom and equatorial to the other. The bridging Cu_2Cl_2 unit is constrained to planarity by the crystallographic inversion center.

The configuration of the $[M(en)_3]^{3+}$ cations (M = Rh, Ir) is always of interest, and a view of the $[Rh(en)_3]^{3+}$ ion is given in Figure 2; the $[Ir(en)_3]^{3+}$ ion has a substantially similar structure. The cation shown in Figure 2 has the $\Delta(\delta\delta\lambda)$ configuration,[19] but in this centrosymmetric space group there is an equal number of enantiomeric $\Lambda(\lambda\lambda\delta)$ forms. For a Δ configuration at the metal, the lowest energy conformer[20] is $\Delta(\lambda\lambda\lambda)$, and this is frequently observed in the solid,[21] although the $\Delta(\delta\lambda\lambda)$ conformer is only slightly more energetic.[22] The present relatively high-energy form has been seen before, however,[9,23,24] and its presence can be attributed to hydrogen-bonding effects involving the amine groups and the chlorine and oxygen atoms. The bond distances and angles in the cations are compared in Table V.

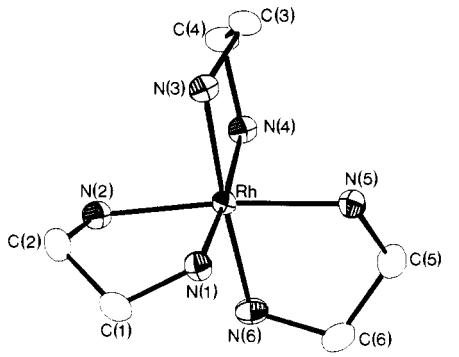

Figure 2. View of the $[Rh(en)_3]^{3+}$ cation. The configuration shown is $\Delta(\delta\delta\lambda)$, but in this centrosymmetric structure there are an equal number of $\Lambda(\lambda\lambda\delta)$ configurations. The λ ring is the central ring (Rh-N(4)-C(4)-C(3)-N(3)-Rh). The hydrogen atoms are not shown.

Table V. Selected Intramolecular Distances and Angles in the $[M(en)_3]^{3+}$ Cations in $[M(en)_3]_2[Cu_2Cl_8]Cl_2 \cdot 2H_2O$

atoms	M = Co[a]	M = Rh	M = Ir
M-N(1)	1.968 (12)	2.077 (2)	2.072 (7)
M-N(2)	1.969 (12)	2.067 (2)	2.083 (6)
M-N(3)	1.950 (13)	2.049 (2)	2.078 (6)
M-N(4)	1.957 (12)	2.062 (2)	2.063 (7)
M-N(5)	1.998 (12)	2.078 (2)	2.090 (5)
M-N(6)	1.973 (13)	2.073 (2)	2.097 (5)
N(1)-C(1)	1.464 (19)	1.478 (4)	1.496 (10)
N(2)-C(2)	1.455 (18)	1.494 (4)	1.482 (10)
N(3)-C(3)	1.499 (20)	1.481 (4)	1.497 (10)
N(4)-C(4)	1.469 (20)	1.488 (4)	1.503 (9)
N(5)-C(5)	1.493 (20)	1.485 (4)	1.476 (9)
N(6)-C(6)	1.448 (18)	1.490 (4)	1.500 (10)
C(1)-C(2)	1.551 (21)	1.508 (4)	1.498 (11)
C(3)-C(4)	1.492 (20)	1.511 (4)	1.496 (10)
C(5)-C(6)	1.519 (22)	1.497 (5)	1.479 (11)
N(1)-M-N(2)	83.5 (5)	82.89 (10)	82.0 (2)
N(1)-M-N(3)	91.3 (5)	92.19 (10)	92.8 (3)
N(1)-M-N(4)	174.8 (5)	174.05 (9)	174.2 (2)
N(1)-M-N(5)	92.6 (5)	92.64 (10)	93.5 (2)
N(1)-M-N(6)	92.8 (5)	93.19 (10)	92.7 (2)
N(2)-M-N(3)	89.8 (5)	89.53 (10)	89.3 (2)
N(2)-M-N(4)	93.6 (5)	94.36 (10)	95.2 (2)
N(2)-M-N(5)	174.9 (5)	173.64 (10)	173.7 (2)
N(2)-M-N(6)	92.7 (5)	93.18 (10)	93.7 (2)
N(3)-M-N(4)	83.3 (5)	82.49 (9)	82.1 (2)
N(3)-M-N(5)	93.4 (5)	95.17 (10)	95.3 (2)
N(3)-M-N(6)	175.3 (6)	174.24 (10)	174.1 (3)
N(4)-M-N(5)	90.6 (5)	90.51 (10)	89.6 (2)
N(4)-M-N(6)	91.6 (5)	92.22 (10)	92.6 (2)
N(5)-M-N(6)	84.3 (5)	82.53 (10)	82.1 (2)
M-N(1)-C(1)	110.9 (9)	108.7 (2)	109.9 (5)
N(1)-C(1)-C(2)	104.4 (13)	107.3 (2)	107.0 (7)
C(1)-C(2)-N(2)	106.1 (12)	108.8 (2)	109.6 (6)
M-N(2)-C(2)	111.6 (8)	108.8 (2)	109.6 (4)
M-N(3)-C(3)	109.1 (9)	108.0 (2)	108.5 (4)
N(3)-C(3)-C(4)	105.3 (13)	108.0 (2)	106.5 (7)
C(3)-C(4)-N(4)	107.6 (12)	107.3 (2)	109.0 (6)
M-N(4)-C(4)	111.4 (9)	110.9 (2)	110.4 (4)
M-N(5)-C(5)	109.1 (9)	108.8 (2)	108.8 (4)
N(5)-C(5)-C(6)	108.5 (13)	108.3 (3)	110.9 (6)
C(5)-C(6)-N(6)	107.6 (13)	108.8 (2)	109.1 (6)
M-N(6)-C(6)	112.7 (10)	109.7 (2)	110.2 (5)

Magnetic Susceptibility. The magnetic susceptibility of a powdered sample of $[Rh(en)_3]_2[Cu_2Cl_8]Cl_2 \cdot 2H_2O$ is plotted as

(19) The notation used is from: *Inorg. Chem.* **1970**, *9*, 1.
(20) Corey, E. J.; Bailar, J. C. *J. Am. Chem. Soc.* **1959**, *81*, 2620.
(21) Veal, J. T.; Hodgson, D. J. *Inorg. Chem.* **1972**, *11*, 597 and references therein.
(22) Gollogly, J. R.; Hawkins, C. J. *Inorg. Chem.* **1970**, *9*, 576.
(23) Enemark, J. H.; Quinby, M. S.; Reed, L. L.; Steuck, M. J.; Walthers, K. K. *Inorg. Chem.* **1970**, *9*, 2397.
(24) Raymond, J. N.; Corfield, P. W. R.; Ibers, J. A. *Inorg. Chem.* **1968**, *7*, 842.

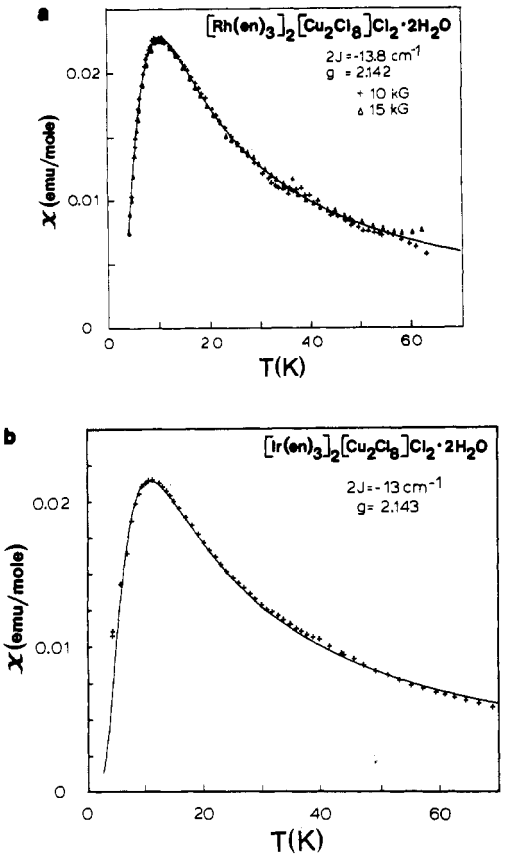

Figure 3. Molar magnetic susceptibility plot vs. temperature for (a) $[Rh(en)_3]_2[Cu_2Cl_8]Cl_2 \cdot 2H_2O$ and (b) $[Ir(en)_3]_2[Cu_2Cl_8]Cl_2 \cdot 2H_2O$.

a function of temperature in Figure 3a. The data, which reflect an antiferromagnetic intradimer coupling of the copper(II) ions, were fitted to the Bleaney–Bowers equation[25]

$$\chi_m = \frac{Ng^2\mu_B^2}{3k(T-\Theta)}[1 + \exp(-2J/kT)/3]^{-1} \qquad (1)$$

with use of a Simplex fitting routine.[26] The g value was taken to be $g = 2.142$, the average value of the **g**-tensor principal components from EPR measurements, and $\Theta = 2ZJ'S(S+1)/3k$. The best fit of the equation to the data yields $2J = -13.8$ cm^{-1}, $g = 2.143$, and $J' = 0.92$ cm^{-1} with $Z = 4$. The solid line in Figure 3a was drawn with use of these parameters. The singlet–triplet splitting $2J$ for the rhodium compound is only slightly lower than that found for the cobalt compound[8] ($2J = -14.6$ cm^{-1}). Susceptibility measurements on a powdered sample of $[Ir(en)_3]_2[Cu_2Cl_8]Cl_2 \cdot 2H_2O$ exhibited unusual behavior. The magnetization value of the powdered sample was very noisy, especially in the 20–40 K temperature range. However, the magnetization of a single crystal (49.8 mg) did not exhibit this unusual behavior, and the magnetic susceptibility data are plotted in Figure 3b along with a solid line calculated from eq 1 with the best-fit parameters $2J = -13.0$ cm^{-1}, $g = 2.143$, and $J' = 0.49$ with $Z = 4$.

EPR Measurements. Crystal *g* Factors. The EPR spectra of single crystals of all three compounds in the *ac* and *ab* planes contain a single Lorentzian line, and neither fine structure nor hyperfine structure are resolved. In the *bc* plane, the EPR spectra contain two lines from copper(II) complexes in magnetically nonequivalent dimers (see Figure 4). Because of orthorhombic crystal symmetry with four symmetrical dimeric units $Cu_2Cl_8^{4-}$ in the unit cell,[9] two EPR lines are also expected in the *ac* and *bc* planes. Crystal structure projections of $[Co(en)_3]_2[Cu_2Cl_8]Cl_2 \cdot 2H_2O$ on the *bc* and *ac* planes are presented in Figure 5. This figure shows that the crystal contains layers of $Cu_2Cl_8^{4-}$ dimers parallel to the *ab* crystal plane at $z = 0$ and $z = 1/2$. The dimers are nearly identically oriented in the layers with the z axis of an individual copper(II) complex (dashed lines in Figure 5) lying very close to the *bc* plane and with an angle $2\theta = 66°$ between the z axes in neighboring layers. Such an arrangement of dimers leads to the conclusion that there are at least two different pathways for interdimer superexchange. Intralayer exchange is stronger than interlayer exchange, and this exchange is responsible for the merging of the fine and hyperfine structure lines into a single Lorentzian line. The value of this interaction in the Co(III) compound has been estimated to be about 0.12 cm^{-1} from the temperature at which fine-structure lines are resolved.[11,12] Interlayer exchange is much smaller because two separate lines are observed in the *bc* plane.

Table VI. Exchange and EPR Parameters of $[M(en)_3]_2[Cu_2Cl_8]Cl_2 \cdot 2H_2O$ Compounds

	M = Co	M = Rh	M = Ir
$2J$, cm^{-1}	−14.8[c]	−13.8	−13.0
J', cm^{-1} [a]	0.12[c]	>0.1	>0.1
J'', cm^{-1} [b] 290 K	0.007 12 (8)	0.001 35 (8)	0.001 90 (8)
77 K	0.003 14 (8)	0.000 70 (5)	0.000 52 (5)
cryst g factors			
g_c	2.227 (3)	2.218 (3)	2.221 (3)
g_b	2.116 (3)	2.109 (3)	2.110 (3)
g_a	2.099 (3)	2.099 (3)	2.098 (3)
molecular g factors[d]			
g_z	2.295 (3) [2.27]	2.290 (3)	2.292 (3)
g_y	2.023 (3) [2.03]	2.020 (3)	2.019 (3)
g_x	2.124 (3) [2.09]	2.116 (3)	2.118 (3)

[a] Intralayer interdimer exchange. [b] Interlayer interdimer exchange. [c] Reference 11. [d] Data in brackets are from reference 11.

The angular dependences of the resonance fields are similar for all three compounds, but the spectra of $[Co(en)_3]_2[Cu_2Cl_8]Cl_2 \cdot 2H_2O$ have the largest line widths, and the spectra of the iridium compound have the smallest line widths. An anisotropy plot for the Rh(III) compound is presented in Figure 6. Angular dpendences of the resonance field are given by eq 2.[27] α, β, and

$$g_i^2(\theta) = \alpha_i + \beta_i \cos 2\theta + \gamma_i \sin 2\theta \qquad (2)$$

γ are anisotropy parameters for the ith crystal rotation, and these were determined by least-squares fitting of eq 2 to a collection of equidistant-angle (10°) experimental points. α, β, and γ are given by[28]

$$\alpha = 1/18 \sum_0^{170°} \mathbf{g}^2(\theta) \qquad \beta = 1/9 \sum_0^{170°} \mathbf{g}^2(\theta) \cos 2\theta$$

$$\gamma = 1/9 \sum_0^{170°} \mathbf{g}^2(\theta) \sin 2\theta$$

The anisotropy parameters collected for the three orthogonal crystal rotations give the components of the $\mathbf{g}^2$ tensor.[29] In these crystals, however, the anisotropy parameters in the *b* and *c* crystal rotations (see Figures 4 and 6) represent the crystal tensors whereas those in the *a* rotation represent the molecular tensor of an individual copper(II) complex. A mathematical averaging of the line positions in the *a* rotation gives the crystal parameters, and standard diagonalization procedure leads to the crystal g factors, the largest g value lying along the crystal *c* axis. The results are summarized in Table VI.

Interdimer Exchange Interaction. The EPR lines observed in the rotational spectra about the *a* axes of the crystals are much broader than the single lines observed in the rotations about the

(25) Bleaney, B.; Bowers, K. D. *Proc. R. Soc. London, Ser. A* **1952**, 214, 451.
(26) See, for example: Hatfield, W. E.; Weller, R. R.; Hall, J. W. *Inorg. Chem.* **1980**, *19*, 3825.
(27) Weill, J. A.; Buch, T.; Clapp, J. E. *Adv. Magn. Reson.* **1973**, *6*, 183.
(28) Hoffmann, S. K.; Corvan, P. J.; Singh, P.; Sethulakshmi, C. N.; Metzger, R. M.; Hatfield, W. E. *J. Am. Chem. Soc.* **1983**, *105*, 4608.
(29) Waller, W. G.; Rogers, M. T. *J. Magn. Reson.* **1975**, *18*, 39.

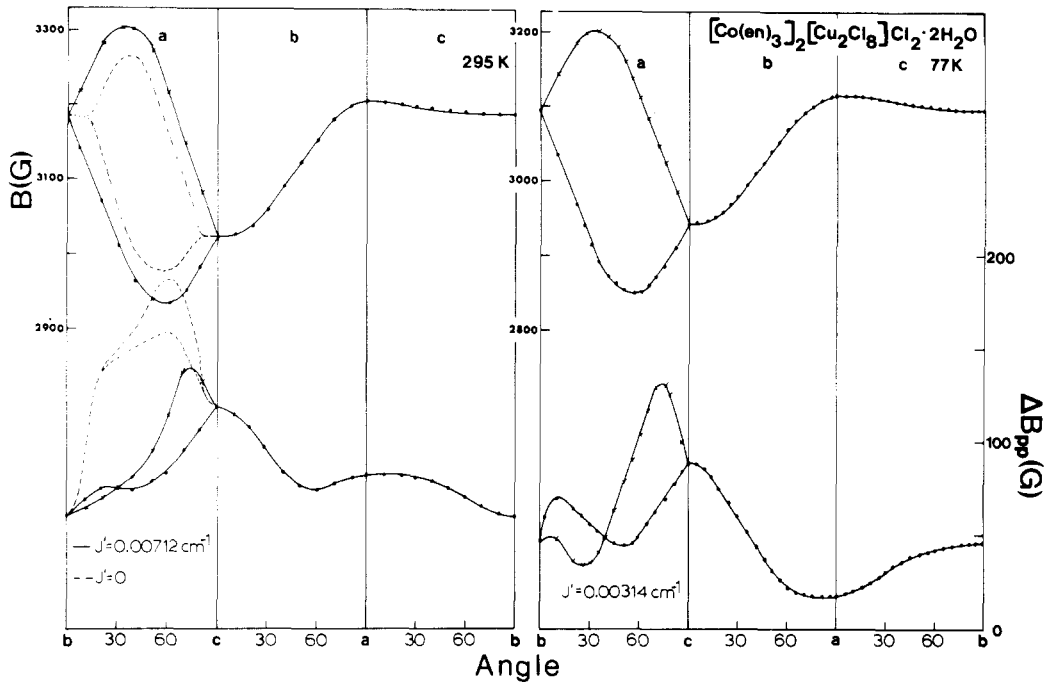

Figure 4. Angular dependence of EPR resonance field and line width at 290 and 77 K for $[Co(en)_3]_2[Cu_2Cl_8]Cl_2 \cdot 2H_2O$. The dashed lines in rotation a represent observed resonance fields perturbed by interdimer coupling. Calculated points on the solid lines were obtained by computer simulation using eq 3. Solid lines on $B(\theta)$ dependences represent the best fit to the anisotropy (eq 2).

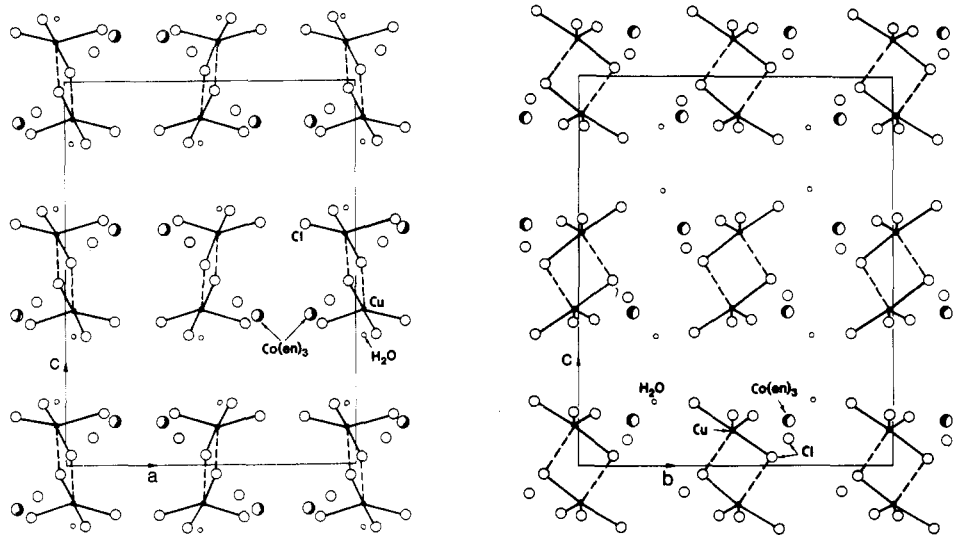

Figure 5. Projections of the structure of $[Co(en)_3]_2[Cu_2Cl_8]Cl_2 \cdot 2H_2O$ on the *bc* and *ac* crystal planes.

other crystal axes. A computer fitting of the two-component spectra to two independent Lorentzian lines gave the resonance fields and line width values, which are plotted by dashed lines in Figure 4 for the Co compound. The fittings, however, are very poor especially in the central part of the spectrum, and it is clear that it is impossible to describe the spectrum as containing two independent lines. This indicates an exchange coupling between magnetically nonequivalent copper(II) dimers that give rise to these lines. In such cases the spectra can be described by a solution of the generalized Bloch equations for interacting paramagnetic centers. For two centers A and B with EPR lines at B^A and B^B having peak-to-peak line widths ΔB^A_{pp} and ΔB^B_{pp} and coupled by an exchange interaction $H'_{ex} = -J' \hat{S}_1 \cdot \hat{S}_2$, the shape of the spectrum is described by eq 3,[30] where the half-width of a line

$$Y(B) = \{N[W_2 - 2(B - B_0)J](W_1^2 + W_2^2) - 4[(B - B_0)W_2 - (\Gamma_0 + 2\Gamma)W_1][(B - B_0)W_1 - (\Gamma_0 + \Gamma)W_2]\}/(W_1^2 + W_2^2)^2 \quad (3)$$

is $\Gamma_i = 3^{1/2}\Delta B^i_{pp}/2$, J (G) = 10967.5J' (cm^{-1}), B_0 and Γ_0 represent average values, and

$$W_1 = (B - B^A)(B - B^B) - (\Gamma_A + J)(\Gamma_B + J) + J^2$$

$$W_2 = (B - B^A)(\Gamma_B + J) + (B - B^B)(\Gamma_A + J)$$

For $J = 0$, eq 3 leads to two Lorentzian lines, and for $J \neq 0$, a merging effect is predicted in the EPR spectrum. A fitting of eq 3 to the experimental spectra for these crystals gives very good agreement between experiment and theory for all crystal orientations, and for all temperatures at which two lines occur in a given spectrum (see Figure 7). The merging of the EPR lines has a significant effect on the EPR spectrum. The lines are strongly broadened and are shifted toward the center of the spectrum, as can be seen in Figure 4, where observed (dashed lines) and calculated (solid lines) resonance fields and line width values are presented. All data in this work were obtained by fitting eq 3 to the spectral data. The interlayer exchange integrals obtained from this fitting procedure at room temperature are $J' = 0.007\,12$ cm^{-1} for the Co(III) compound, $J' = 0.001\,35$ cm^{-1} for the Rh(III)

(30) Hoffmann, S. K. *Chem. Phys. Lett.*, in press.

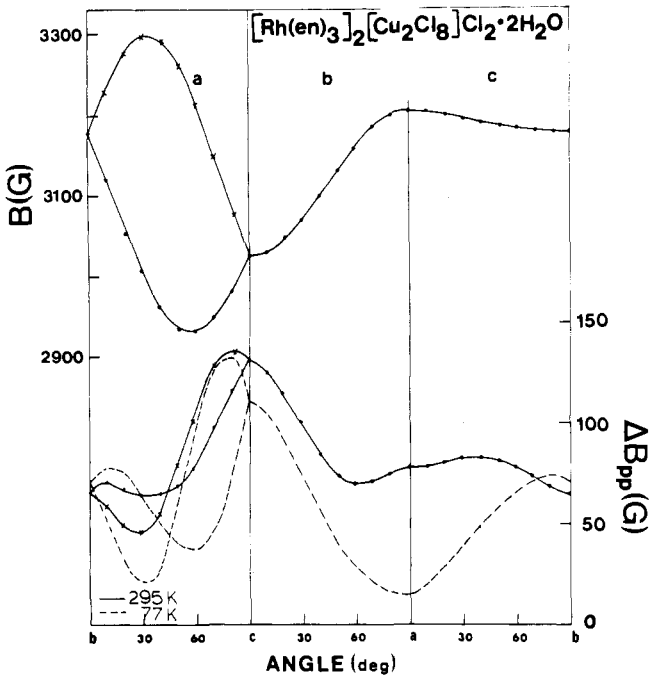

Figure 6. Angular dependence of the EPR resonance field and line width of $[Rh(en)_3]_2[Cu_2Cl_8]Cl_2 \cdot 2H_2O$. The resonance fields are temperature independent, but the line width decreases with temperature for most orientations as shown by the dashed line at 77 K.

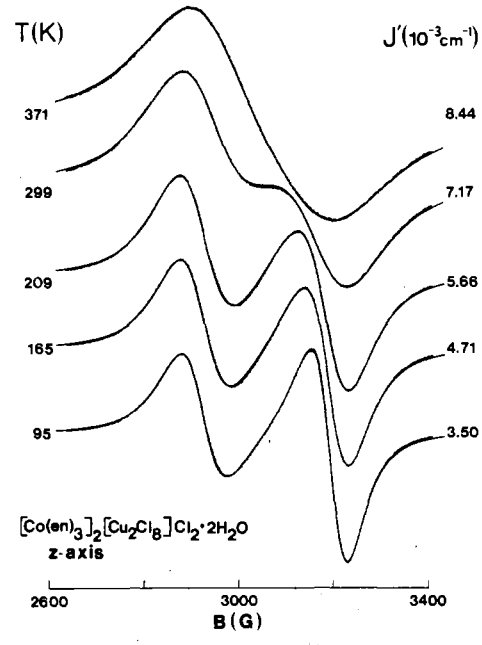

Figure 7. The temperature dependence of the EPR spectra of $[Co(en)]_2[Cu_2Cl_8]Cl_2 \cdot 2H_2O$ observed along the molecular z axis. Solid lines, which superimposed perfectly on experimental spectra, were calculated from eq 3 with interdimer-exchange integrals J' indicated on the spectra.

compound, and $J' = 0.001\,90$ cm^{-1} for the Ir(III) compound (see Table VI). Thus, the exchange interaction between the copper(II) dimers in neighboring layers is larger in $[Co(en)_3]_2[Cu_2Cl_8]Cl_2 \cdot 2H_2O$ than in the other two compounds.

Interlayer exchange determined from analysis of the EPR data does not agree with the θ values from the analysis of the magnetic susceptibility data. The Θ value in eq 1 is a curve-fitting parameter that reflects other phenomena such as a temperature dependence in the singlet–triplet splitting, and a correlation is not expected.

Molecular *g* Factors. The parameters g_c, g_b, and g_a in Table VI represent principal values of the averaged **g** tensor of a crystal with principal directions along the crystallographic axes. Molecular g factors describing the electronic structure of individual

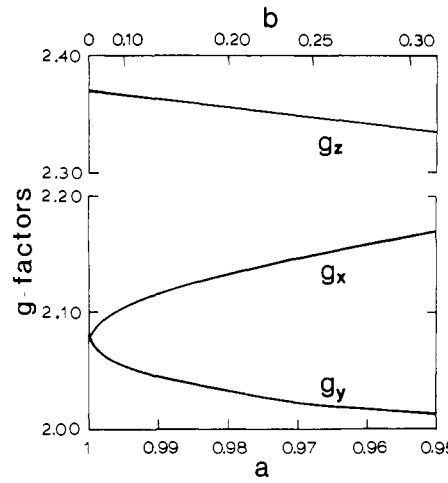

Figure 8. Dependence of g_z, g_y, and g_x on orbital mixing coefficients in the ground state of the Cu(II) ion, $a(d_{x^2-y^2}) + b(d_{z^2})$, with $E_{xy} = 13\,000$ cm^{-1}, $E_{xz} = 16\,000$ cm^{-1}, $E_{yz} = 17\,000$ cm^{-1}, and $\lambda_{eff} = -650$ cm^{-1}.

copper(II) complexes can be found by a general mathematical decoupling procedure[31] from crystal g factors and the angles of the mutual orientation of the nonequivalent complexes.

The z-axis direction is expected to be close to the $Cu-Cl_{apical}$ direction in the copper(II) complex, but because of the low crystal symmetry of the complex some deviation can exist. Moreover, the g_z value must be very close to the maximal g-factor value observed in the crystal a rotation since the $Cu-Cl_{apical}$ direction lies nearly in the crystal bc plane. The direction of the x axis is not determined by a Cu–ligand direction in low-symmetry complexes. The resulting molecular g factors are summarized in Table VI. The results show similar **g** tensors in all three crystals with the crystal x axes perpendicular to the plane containing the molecular z axes of the copper(II) ions in nonequivalent dimers. The molecular g factors collected in Table VI also indicate a nonaxial crystal field of the complexes with the ground-state wave function being mainly $d_{x^2-y^2}$ in a distorted-square-pyramidal stereochemistry. The g values suggest that the ground-state wave functions contain an admixture of excited orbital states.[32] A lowering of symmetry from C_{4v} to C_{2v} results in identical symmetries of $d_{x^2-y^2}$ and d_{z^2} orbitals. Thus, the excited state d_{z^2} can be mixed into the ground state and the resulting wave function of the copper(II) ion can be written as

$$\psi = a(d_{x^2-y^2}) + b(d_{z^2}) \qquad a^2 + b^2 = 1 \tag{4}$$

The admixture of the d_{z^2} is not expected to be very large and can be determined from molecular g factors with use of eq 5, where

$$g_z = 2 - 8a^2\lambda/E_{xy} \qquad g_y = 2 - 2(a - 3^{1/2}b)^2\lambda/E_{xz}$$
$$g_x = 2 - 2(a + 3^{1/2}b)^2\lambda/E_{yz} \tag{5}$$

λ is the effective spin–orbit coupling parameter ($\lambda = k\lambda_0$ with the orbital reduction factor $k = 0.5$–1.0 and $\lambda_0 = -829$ cm^{-1} for free Cu(II) ion). The E_{ij} values are the energies of the d_{ij} orbital states with respect to the ground state. These orbital energies are unknown for these compounds, and it is impossible to solve eq 5 uniquely. It is reasonable to expect that the difference $E_{yz} - E_{xz}$ is not very large, and by taking $E_{xz} = E_{yz}$ the mixing coefficients can be estimated. Solutions of eq 5, together with the normalization condition in eq 4, gives the wave functions

Co compound: $\psi_{gs} = 0.979(d_{x^2-y^2}) + 0.204(d_{z^2})$

Rh compound: $\psi_{gs} = 0.978(d_{x^2-y^2}) + 0.209(d_{z^2})$

Ir compound: $\psi_{gs} = 0.977(d_{x^2-y^2}) + 0.213(d_{z^2})$

(31) Hoffmann, S. K.; Szczepaniak, L. S. *J. Magn. Reson.*, in press.
(32) Hathaway, B. J.; Billing, D. E. *Coord. Chem. Rev.* **1970**, *5*, 142.

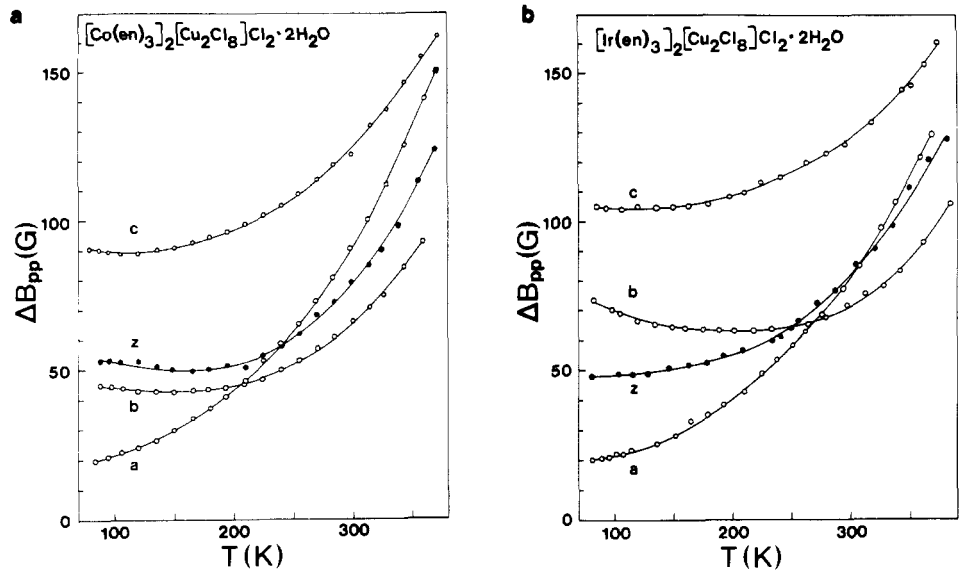

Figure 9. Temperature dependence of the line width observed along crystallographic axes and along the molecular z axis: (a) $[Co(en)_3]_2[Cu_2Cl_8]Cl_2 \cdot 2H_2O$; (b) $[Ir(en)_3]_2[Cu_2Cl_8]Cl_2 \cdot 2H_2O$.

All of the compounds have similar electronic structures.

An admixture, even small, of the d_{z^2} state into ground state $d_{x^2-y^2}$ results in a changing of the "normal" g-factor sequence $g_x > g_y > g_x$ to $g_z > g_x > g_y$. The change takes place when

$$(a + 3^{1/2}b)^2E_{xz} > (a - 3^{1/2}b)^2E_{yz}$$

and occurs for b values larger than about 0.03. The g-factor dependence on the mixing coefficients is presented in Figure 8 for typical parameters of Cu(II) complexes. This figure clearly indicates that a large nonaxiality of the molecular **g** tensor can be due to orbital mixing, with a resulting g_y value close to the free-electron value (g_e = 2.0) for relatively large admixtures.

Temperature Dependence of the EPR Spectra. Within experimental error the crystal g factors and molecular g factors are temperature independent in the range 77–380 K. However, temperature affects the line width value and the strength of the exchange coupling. The temperature dependence of the EPR spectrum of $[Co(en)_3]_2[Cu_2Cl_8]Cl_2 \cdot 2H_2O$ observed along the molcular z axis is presented in Figure 7. Fitted spectra from eq 3 and the resulting interlayer exchange integral are also given. It may be seen that the lines broaden and the exchange coupling increases with increasing temperature. There is a complete merging of the lines at about 380 K. Temperature variations of the line width in the Co and Ir compounds are presented in parts a and b, respectively, of Figure 9. The temperature dependence of the line width for the Ir compound is very similar to that in the Rh compound.

The lines are broad at high temperatures and exhibit a narrowing with decreasing temperature, an effect that differs in different crystal directions. The line width is expected to have two dipolar contributions, these coming from inter- and intradimer dipolar coupling. The former one is calculated to be about 20 G from the point-dipole approximation using the 9.95-Å distance between copper(II) dimers in layers. This contribution is small, but it probably determines the line width along the a axis at 77 K (see Figure 9). Intradimer dipole coupling is much larger and is predicted to be about 400 G along the Cu–Cu direction. This zero-field splitting is not resolved in the temperature range 77–380 K, but it does determine the line width value, since the maximum line width is along the crystal c axis, which is close to the Cu–Cu intradimer direction (see Figure 5). The increase in the ΔB_{pp} value at low temperatures, as observed along the b axis (Figure 9), reflects a beginning of the fine-structure resolution. The fine structure is fully resolved below 15 K in the Co compound.[11]

Temperature Dependence of the Interdimer Exchange. Superexchange coupling between nonequivalent dimers in neighboring layers in the compounds decreases strongly with temperature as

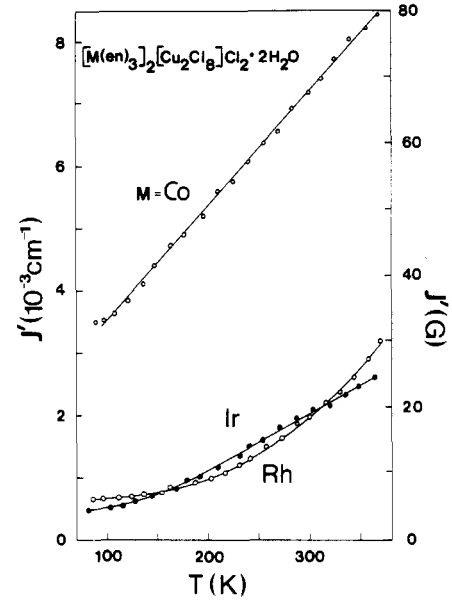

Figure 10. Temperature dependence of interdimer exchange between magnetically nonequivalent dimers in $[M(en)_3]_2[Cu_2Cl_8]Cl_2 \cdot 2H_2O$ (M = Co, Rh, Ir) compounds.

can be seen from Figure 10. There is a linear decrease of J' values in the Co compounds, and nonlinear behavior is observed in the IR and Rh compounds. This behavior is opposite to that expected from thermal crystal lattice contractions. A lattice contraction can result in interionic distances shortening, and this should lead to an increase in exchange coupling. For example, in $K_2CuCl_4 \cdot 2H_2O$ the exchange integral increases from 0.09 cm^{-1} at 300 K to 0.17 cm^{-1} at 77 K.[33-35] An increase in the intradimer coupling with decreasing temperature has been found in $[Cu_2(tren)(OCN)_2](BPh_4)_2$ and $[Cu_2(tren)_2(SCN)_2](BPh_4)_2$ from direct observation of singlet–triplet transitions in the EPR spectra.[36] A small increase in intradimer exchange coupling with decreasing temperature has been observed in optical and luminescence spectra of $[Cr_2(OH)_2(en)_4]I_4$[37] and in inelastic neutron

(33) Zaspel, C. E.; Drumheller, J. E. *Phys. Rev. B: Solid State* **1977**, *18*, 1771.
(34) Okuda, T.; Date, M. *J. Phys. Soc. Jpn.* **1970**, *28*, 308.
(35) Kennedy, T. A.; Sung Ho Choh; Seidel, G. *Phys. Rev. B: Solid State* **1971**, *2*, 3645.
(36) Duggan, D. M.; Hendrickson, D. N. *Inorg. Chem.* **1974**, *13*, 2929.

scattering in $[Cr_2(OH)(NH_3)_{10}]Cl_5 \cdot H_2O$.[38] The failure of standard theoretical models to fit experimental magnetic susceptibility data for $(C_7H_7NH_3)_2MnCl_4$, $(C_7H_7NH_3)MnBr_4$,[39] and $Cu(n\text{-}C_3H_7nso)NO_3$[40,41] has been explained as a result of an increase in exchange coupling with decreasing temperature.

A decrease of the exchange integral with a decrease in temperature was determined by EPR in $[N(n\text{-}Bu)_4]_2[Cu(mnt)_2]$.[42] The exchange integral in this compound is nearly constant above 200 K ($\sim$0.04 cm^{-1}), below which J' decreases strongly with temperature. Magnetic susceptibility measurements on binuclear copper(II) cryptates yield $2J = -57$ cm^{-1} above 50 K, but exchange coupling decreases rapidly at low temperatures.[43]

The decrease of interdimer superexchange interaction with temperature in these crystals probably is a result of dynamical crystal lattice properties. Exchange interactions are expected to be proportional to overlap integrals between atomic orbitals in the superexchange pathways. The overlapping of orbitals is modulated by thermal lattice vibrations and depends on the average amplitude of atomic displacements, which are temperature dependent. The mean-square displacement of atoms $\langle \mu^2 \rangle$ varies linearly[44,45] with temperature in the high-temperature region, where coth $(\hbar\omega/2kT) \approx 2kT/\hbar\omega$ ($\hbar\omega$ is the energy of a normal mode of a lattice vibration). Thus, the temperature dependence of interdimer exchange can be related to $\langle \mu^2 \rangle$, as has been observed for the g factor in a HgSe:Mn^{2+} single crystal[33] and for the isotropic hyperfine splitting of Cu^{II} and vanadyl complexes in solutions.[46,47]

Conclusions

The compounds presented in this paper have similar crystal and molecular structures and magnetic properties. The differences in the intradimer exchange coupling in $Cu_2Cl_8^{4-}$ units reflect small differences in chloride bridge geometry. The electronic structures of individual Cu(II) complexes in the three compounds have ground states containing the mixed orbitals $\psi_{gs} = 0.98(d_{x^2-y^2}) + 0.2(d_{z^2})$. The main differences observed in the EPR spectra of these compounds result from differences in interdimer exchange coupling. Interdimer coupling is about 3 orders of magnitude smaller than intradimer coupling, but it produces a broadening and a shift of the EPR lines.

The temperature behavior of the interdimer exchange integral J' in these compounds reflects dynamical properties of the crystal lattice. In general, however, the problem of the temperature dependence of the exchange integral is complicated, and there are differences both in the sign and in the shape of dJ/dT in the systems that have been studied. The crystal lattice contraction effect on dJ/dT and a phonon modulation of orbital overlapping can produce effects of opposite sign. An anisotropy in the lattice contraction and more than one superexchange pathway can complicate the situation even more. Significant effects are produced by exchange elasticity phenomena,[43] where competition between elastic crystal energy and exchange coupling can determine an equilibrium state of the crystal lattice or molecular structure of a paramagnetic cluster. In crystals where the ground state of the cluster is diamagnetic, as it is in the case of antiferromagnetically coupled Cu(II) dimers, the interdimer exchange coupling is expected to be proportional to the probability that nearest neighbors are in excited paramagnetic states.[48,49] This dependence can influence J' values for temperatures lower than the singlet–triplet splitting, although definite experimental evidence does not exist to support this contention.

Acknowledgment. This research was supported by the National Science Foundation (Grant No. CHE 8308129) and the Petroleum Research Fund, administered by the American Chemical Society.

Registry No. I, 28852-88-2; II, 86751-15-7; III, 86959-84-4.

Supplementary Material Available: Listings of hydrogen atom positional parameters, anisotropic thermal parameters, and observed and calculated structure factors (45 pages). Ordering information is given on any current masthead page.

(37) Beutler, A.; Güdel, H. U.; Snellgrove, T. K.; Chapuis, G.; Schenk, K. *J. Chem. Soc., Dalton Trans.* **1979**, 983.
(38) Güdel, H. U.; Furrer, A. *Mol. Phys.* **1977**, *33*, 1335.
(39) Groenendijk, H. A.; Duyneveldt, A. J.; Willett, R. D. *Physica B+C (Amsterdam)* **1979**, *98B+C*, 53.
(40) Mikuriya, M.; Okawa, H.; Kida, S. *Bull. Chem. Soc. Jpn.* **1982**, *54*, 2979.
(41) Nakatsuka, S.; Osaki, K.; Uryu, N. *Inorg. Chem.* **1982**, *21*, 4332.
(42) Plumlee, K. W.; Hoffman, B. M.; Ibers, J. A.; Soos, Z. G. *J. Chem. Phys.* **1975**, *63*, 1926.
(43) Kahn, O.; Morgenstern-Badarau, I.; Audiere, J. P.; Lehn, J. M.; Sullivan, S. A. *J. Am. Chem. Soc.* **1980**, *102*, 5935.
(44) Willis, B. T.; Pryor, A. W. "Thermal Vibrations in Crystallography"; Cambridge University Press: New York, 1975.
(45) Shrivastava, K. N. *J. Phys. C.* **1982**, *15*, 3869.
(46) Baranov, D. G.; Zhytnikov, R. A.; Melnikov, N. I. *Phys. Status Solidi* **1969**, *33*, 463.
(47) Bylinskaya, L. A.; Kozyrev, B. M.; Ovchinnikov, I. V. *Magn. Reson. Relat. Phenom., Proc. Congr. Ampere* **1977**, *17*, 1000.
(48) Soos, Z. G. *J. Chem. Phys.* **1966**, *44*, 1729.
(49) McGregor, K. T.; Soos, Z. G. *Inorg. Chem.* **1976**, *15*, 1976.

Contribution from the School of Chemistry,
University of New South Wales, Kensington, NSW 2033, Australia

c-$Ni_8(SCH_2COOEt)_{16}$, a Receptive Octagonal Toroid

IAN G. DANCE,* MARCIA L. SCUDDER, and RODNEY SECOMB

Received July 2, 1984

The red compound $Ni(SCH_2COOEt)_2$, prepared by interaction of ethyl 2-mercaptoacetate with nickel salts in basic solution, is unusually soluble in a variety of inert solvents. The crystals contain cyclic molecules $Ni_8(SCH_2COOEt)_{16}$ in which eight NiS_4 rectangular coordination planes (Ni–S = 2.19 Å; S–Ni–S = 82.4, 98.3°) constitute an octagonal prism. The approximate molecular symmetry is C_{8h} for the Ni_8S_{16} core and D_{4d} when the axial and equatorial S–C bonds are included, while the array of externally pendant ligand tails is asymmetric. The Ni···Ni diameters of the toroidal molecule range from 7.6 to 8.3 Å; S···S diameters range from 8.0 to 9.6 Å. This allows sufficient space for inclusion (van der Waals or coordinative) of small molecules, and the tail of one axial ligand returns to enter the octagon with the ethyl group on the toroid axis and weak ester oxygen coordination to two adjacent nickel atoms (O–Ni = 3.0 Å). Inclusion of added species has not been detected. The detailed dimensions of the metal coordination and the hinged bridge in this first example of a cyclic $M_8(SR)_{16}$ molecule are evaluated in comparison with those of known $M_6(SR)_{12}$ and $M_4(SR)_8$ cyclic molecules. Crystal data: space group $P\bar{1}$, $a = 13.367$ (2) Å, $b = 29.500$ (3) Å, $c = 29.818$ (3) Å, $\alpha = 61.64$ (1)°, $\beta = 81.46$ (1)°, $\gamma = 81.35$ (1)°, $Z = 4$, $d_{obsd} = 1.56$ g cm^{-3}, $d_{calcd} = 1.55$ g cm^{-3}, $R = 0.088$ for 8997 observed reflections.

Introduction

Compounds $M(SR)_2$ of the metals Ni, Pd, and Pt where R does not contain solubilizing functions are generally insoluble in inert solvents. Accordingly, one-dimensionally nonmolecular structures were proposed for these compounds by Jensen[1] in 1944, and have been assumed since, but have not been confirmed by diffraction

(1) Jensen, K. A. *Z. Anorg. Allg. Chem.* **1944**, *252*, 227.

0020-1669/85/1324-1201$01.50/0